Modeling and Simulation of the Operating Zero Point of Voltage Sensors

Ye He
Electronic and Information Engineering College of Physical Science and Technology, Central China Normal University, Wuhan 430079, Hubei, China
Corresponding author: Ye He (e-mail: heye147741@163.com).

ABSTRACT Compared to isolation amplifier voltage sensors and magnetic balance voltage sensors, magnetic modulation voltage sensors exhibit higher measurement accuracy and faster response time, and are widely used in fields such as leakage current monitoring and AC drive torque control. The verification of magnetically modulated voltage sensors mainly relies on physical experiments, which is time-consuming, labor-intensive and inefficient in design. To address this issue, this paper establishes a circuit simulation model of the magnetic core. The variations in zero offset and zero drift of the voltage sensor are analyzed under different parameters of the magnetically modulated core and mutual-inductance core, respectively, and corresponding rules are summarized. The simulation results show that zero offset is related to the voltage at the junction of the two secondary coils. The higher the voltage at this junction, the greater the current flowing to the output terminal, and the larger the zero offset. And zero drift is related to frequency, matching capacitance, and the inductance of the second magnetic core. This work can provide effective theoretical guidance for the design of high-precision magnetically modulated voltage sensors, which can greatly save time in design.

INDEX TERMS magnetic modulation, permeability, voltage sensor, zero offset, zero shift

I. INTRODUCTION

C urrently, isolated amplification voltag sensors, magnetic balance voltage sensors, and magnetically modulated voltage sensors are the main types applied in railway locomotives and metro vehicles [1-5]. Among them, isolated amplification voltage sensors detect the magnetic field signal generated by the primary current at the air gap and then process the detected signal. Although they have advantages such as compact structure, simple circuit, and low power consumption [6-9], their measurement range is relatively narrow. Magnetic balance voltage sensors balance the magnetic flux generated by the primary current with the magnetic flux generated by the secondary current through the secondary winding, and measure the primary current by detecting the secondary current. They feature excellent heat dissipation design and superior electromagnetic compatibility [10-14]. However, due to the large number of turns and high inductance of the primary and secondary windings, the output response time is long, generally ranging from 50 to 70 microseconds. In comparison, magnetically modulated voltage sensors utilize the alternating saturation characteristic of high-permeability magnetic cores under internal square-wave voltage excitation, enabling rapid modulation of the primary current signal to the secondary winding via the ampere-turn balance principle. This allows the secondary winding output current to accurately follow the variation of the primary current signal, thus achieving extremely fast response speed and high accuracy [15-16].

In the previous design and fabrication of magnetically modulated voltage sensors, designers primarily verified the feasibility of design schemes by fabricating prototypes and conducting a series of tests, which consumed considerable time and effort [17-18]. In this paper, we perform simulation analysis of the zero offset of magnetically modulated voltage sensors through magnetic core modeling. This approach can provide a theoretical basis for product design and significantly reduce design time.

II. MATERIALS AND METHODS

A. WORKING PRINCIPLE OF THE MAGNETICALLY MODULATED VOLTAGE SENSOR

The basic principle block diagram of the magnetically modulated voltage sensor is shown in Fig. 1. Magnetic core I (modulation core), together with coil L1, the RC circuit, and the square-wave generator N1, forms the self-excited oscillation circuit, which serves as the core of the magnetic modulation function [19].

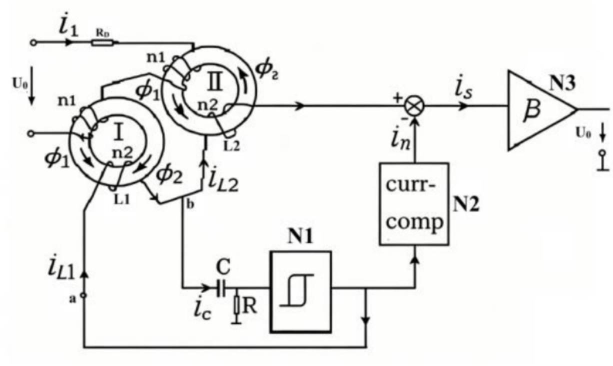

FIGURE 1. Block diagram of operating principle for magnetic modulation voltage sensor

The square-wave generator N1 outputs a symmetric square-wave voltage to drive magnetic core I into alternating deep magnetic saturation in the positive and negative half-cycles. The high-permeability core's nonlinear saturation characteristic modulates the DC/low-frequency magnetomotive force generated by the measured primary current i1 onto a high-frequency square-wave carrier.

When the core enters saturation, the peak current of coil L1 triggers N1 to flip its output polarity, maintaining the self-excited oscillation and providing a stable modulation excitation for the entire sensor.

The measured voltage u_1 is converted into the primary current i_1 through the current-limiting resistor R_D, which generates a magnetomotive force in magnetic core I, changing the saturation timing and depth of the core. This process loads the measured signal onto the oscillation waveform, realizing signal extraction under electrical isolation.

Magnetic core II (mutual-inductance core) forms a dual-core coupling structure with Magnetic Core I, realizing mutual-inductance coupling and current compensation to ensure ampere-turn balance and zero-point optimization.

The primary current i_1 generates a co-directional magnetomotive force in both magnetic cores, and the secondary coil L2 induces the corresponding current i_{L2}, realizing signal transmission and electrical isolation between the primary and secondary sides.

Cooperating with the current compensation module N2, it compensates for the excitation current and saturation peak current of magnetic more I, making the combined secondary current $i_{L2} + i_n$ accurately follow the primary current i_1, satisfying the ampere-turn balance principle and greatly improving measurement accuracy.

The current i_{L2} flowing through coil L2 and the current i_1 generate a co-directional magnetomotive force, keeping magnetic core II in a continuous saturated state, stabilizing the mutual-inductance coupling characteristic, suppressing zero drift, and significantly improving the response speed of the sensor (far faster than traditional magnetic balance voltage sensors).

The two magnetic cores with symmetric winding turns (n_1, n_2) realize the closed-loop operation of "modulation-compensation-demodulation" through the coupling of magnetic flux ϕ_1 and ϕ_2: magnetic core I completes the modulation of the measured signal, magnetic core II realizes compensation and coupling for ampere-turn balance and signal isolation, and finally, the amplifier N3 demodulates and outputs the voltage u_0 linearly corresponding to the input voltage u_1. This dual-core structure is the core design for the magnetically modulated voltage sensor to achieve high response speed, high accuracy, and strong anti-interference ability, which is especially suitable for complex electromagnetic environments such as rail transit and power systems.

B. ZERO-POINT SIMULATION

The circuit model of magnetic modulation voltage sensor is established in this paper, which mainly includes two magnetic cores, first core and second core [20]. The first magnetic core refers to the core functioning for magnetic modulation; the second magnetic core refers to the core functioning for mutual inductance.

Even when the measured quantity is zero, there is always a certain voltage difference at the op-amp input between the connection points of the two secondary coils. As a result, the voltage at the connection point of the two secondary coils is not zero, the current flowing to the output terminal is not zero, and the final output voltage is consequently non-zero, indicating the existence of zero offset [21].

To analyze the factors influencing the zero point, simulations are carried out under an uncalibrated state, and the zero offset and zero drift are obtained by observing the output.

1) CHANGE OF THE SECOND MAGNETIC CORE

With other parameters kept constant, the permeability of the second magnetic core (i.e., the inductance) is varied, and the zero offset and zero drift are observed.

2) OUTPUT WAVEFORM WHEN THE INDUCTANCE OF THE SECOND MAGNETIC CORE CHANGES

The inductance values of the second magnetic core are 0.03 mH, 0.1mH, and 1mH, respectively. Output zero-point waveforms when the inductance of the second magnetic core is set to the original parameter (black, consistent with the first magnetic core), 0.03 (red), 0.1 (green), and 1 (blue), respectively. Among them, (a) and (b) are the superimposed and separated plots, and (c) and (d) are the enlarged plots. The simulation results are shown in Fig. 2.

3) OUTPUT DATA WHEN THE INDUCTANCE OF THE SECOND MAGNETIC CORE VARIED

Zero bias and zero drift when the inductance of the second magnetic core is set to the original parameter (consistent with the first magnetic core), 0.03mH, 0.1mH, and 1mH, respectively. The summary of zero bias and zero drift results is shown in Table1. It can be seen that as the inductance increases, the zero bias changes slightly, while the zero drift decreases.

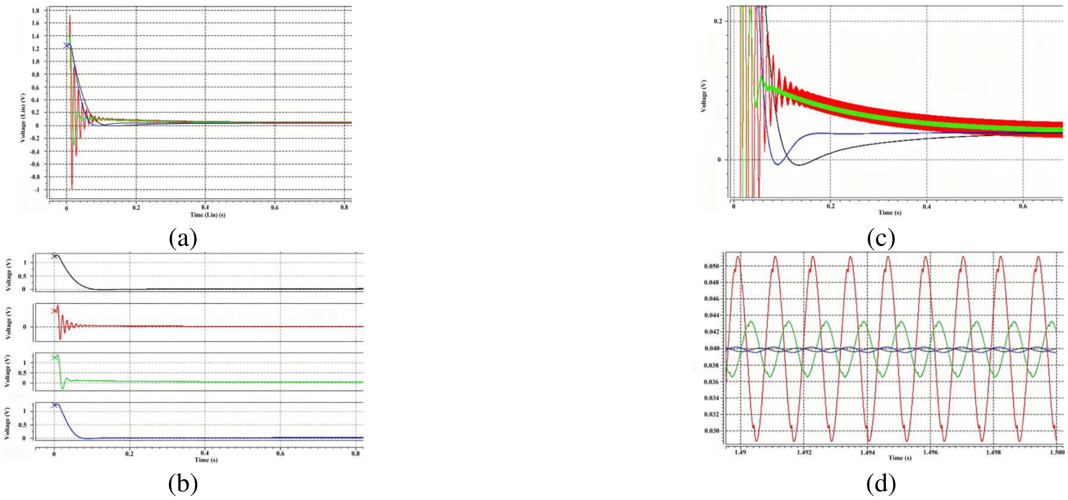

FIGURE 2. Zero-bias and zero-drift output waveforms under different inductance values

TABLE 1. Summary of Zero Bias and Zero Drift Results Under Different Inductance Values

Items	Original parameters	$L = 0.03$ mH	$L = 0.1$ mH	$L = 1$ mH
Zero bias/mV	39.818	39.92	39.91	39.8332
Zero drift/mV	0.436	22.36	6.72	0.6686

C. CHANGE OF FIRST CORE

1) MAGNETIC CORE PARAMETERS

A simplified magnetic core model, though deviating considerably from the real one, is adopted for preliminary simulation of zero drift and zero offset, so as to roughly identify their ranges and patterns.

where Rmu, H0, H1, A0 and A1 are parameters of the magnetic core model. Their specific values are obtained by fitting the magnetization curve of the actual magnetic core. There is no explicit mathematical relationship between the fitting parameters and parameters such as permeability derived from the magnetization curve. If the initial values of the four magnetic cores a, b, c and d are close to each other during fitting, the larger the permeability, the larger the resulting fitting parameter Rmu.

2) ZERO OFFSET AND ZERO DRIFT WITH THE SAME MAGNETIC FLUX

The magnetization curves of magnetic cores b, c, and d, obtained using the magnetic core parameters listed in table 2, are shown in Fig. 3. By adjusting djusting the relevant parameters, the magnetic flux of the three magnetic cores b, c, and d is kept consistent. The simulation zero points of the three magnetic cores are shown in Fig. 4.

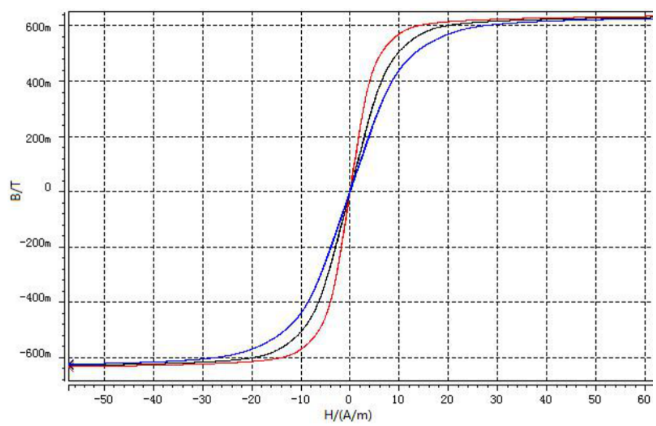

FIGURE 3. Magnetization curves for different magnetic core parameters: b (red), c (black), d (blue)

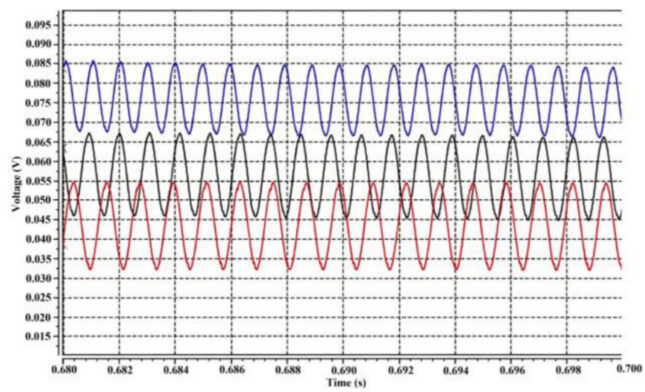

FIGURE 4. Zero points of cores with different permeabilities: b (red), c (black), d (blue)

3) ZERO OFFSET AND ZERO DRIFT UNDER THE SAME SATURATION MAGNETIC FIELD HS

By varying the magnetic core thickness while keeping the saturation magnetic field Hs constant, the saturation magnetic flux is changed. Taking magnetic core b as an example,

TABLE 2. Core Parameters Corresponding to Different Permeabilities

Magnetic Core Number	Actual Permeability	Rmu	H0	H1	A0	A1
a	0.20374	0.325687818527067	0.00176415070542192	$4.61231882871974 \times 10^{-29}$	0.11975419926149	0.0144011836437372
b	0.1134	0.180961975226093	0.00293071341901896	$9.64519302695765 \times 10^{-28}$	0.119547863039	0.0149957469528492
c	0.06831	0.108632863257483	0.00359372340361825	$3.79553081685608 \times 10^{-27}$	0.119389949115541	0.0152491626671055
d	0.05174	0.0821868456378383	0.00501389027487910	$1.60489855765469 \times 10^{-26}$	0.118511448726748	0.0155550640305455

the relationship between magnetic flux and magnetic field as well as the simulation zero point are shown in Fig. 5 and Fig. 6, respectively.

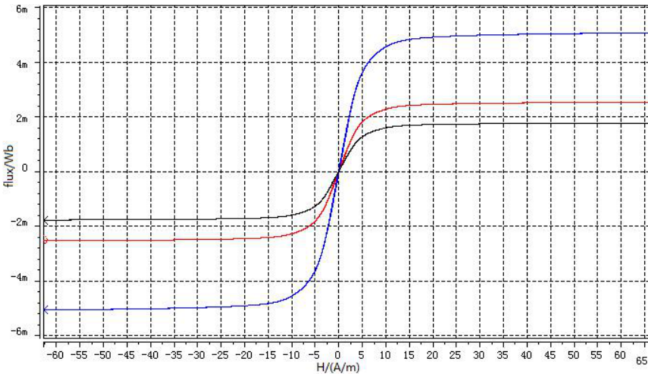

FIGURE 5. Flux vs. magnetic field curves at the same saturation magnetic field: unchanged thickness (red), 0.7× increased thickness (black), 2× increased thickness (blue)

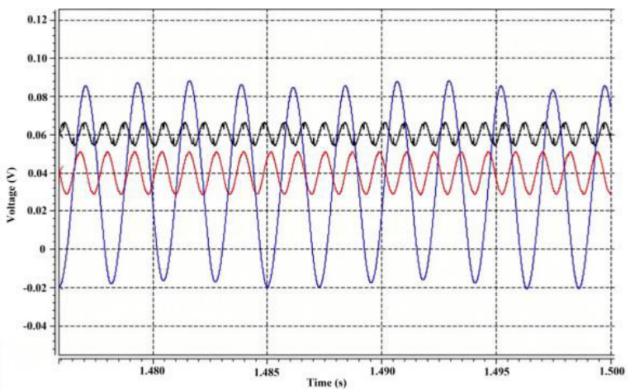

FIGURE 6. Zero points of magnetic cores at the same saturation magnetic field: unchanged thickness (red), 0.7× thickness increase (black), 2× thickness increase (blue)

4) ZERO OFFSET AND ZERO DRIFT AT THE SAME INDUCTANCE L (MAGNETIC CORES LABELED B, C, D RESPECTIVELY)

By adjusting the thickness of magnetic cores c and d to make their inductance L equal to that of core b, the saturation magnetic flux is varied. The relationship between magnetic flux and magnetic field, as well as the simulation zero point, are shown in Fig. 7 and Fig. 8, respectively.

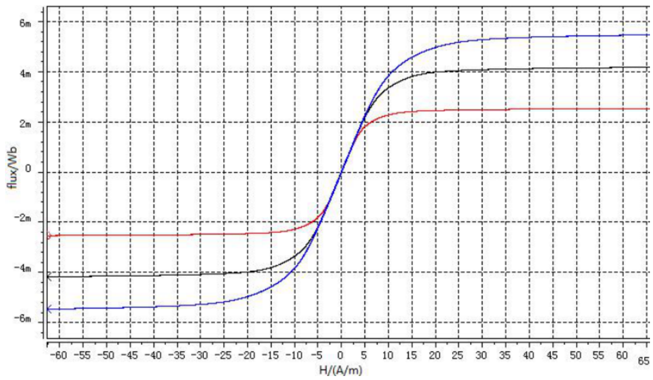

FIGURE 7. Flux vs. magnetic field curves at the same inductance: unchanged thickness of core b (red), 1.6584× thickness increase of core c (black), 2.1836× thickness increase of core d (blue)

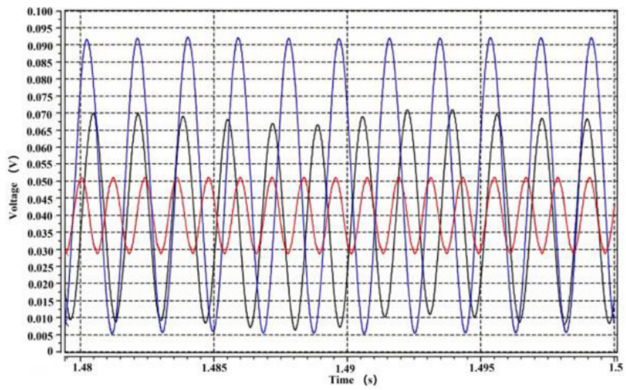

FIGURE 8. Zero points at the same inductance: unchanged thickness of core b (red), 1.6584× thickness increase of core c (black), 2.1836× thickness increase of core d (blue)

5) OUTPUT DATA WHEN THE FIRST MAGNETIC CORE VARIED

The output data of voltage sensor varying with the first magnetic core is shown in Table 3.

TABLE 3. Output Data When the First Magnetic Core Varied

	Same Hs (by Varying the Thickness of Magnetic Core b)			Same L (by Varying the Thickness of Magnetic Cores b, c, and d)			Same Magnetic Flux		
	Thickness (3.5mm)	Thickness (5mm)	Thickness (10mm)	Thickness (b, 5mm)	Thickness (c, 8.3mm)	Thickness (d, 10.9mm)	b	c	d
Zero Point/mv	60.45	39.9	34.15	39.9	38.075	48.67	39.9	49.15	63.1
Zero Drift/mv	12.3	22.4	108.3	22.4	60.65	86.06	22.4	21.5	18.2
Frequency/Hz	1142.86	840.689	440.141	840.689	594.884	529.241	840.689	925.926	1020.41

III. RESULTS AND DISCUSSION

Zero offset is related to the voltage at the junction of the two secondary coils. The higher the voltage at this junction, the greater the current flowing to the output terminal, and the larger the zero offset. The voltage at the junction of the two secondary coils is the difference between the excitation voltage and the coil induced voltage. The excitation amplitude remains constant, while the coil induced voltage depends on the magnetic core.When Hs is constant, as the inductance L increases, the induced voltage of the secondary coil increases, resulting in a smaller zero offset.When the magnetic flux is constant, as Hs increases, the secondary induced voltage decreases, leading to an increase in zero offset.When L is constant, as Hs and magnetic flux increase, magnetic core saturation becomes more difficult, the frequency decreases (with L unchanged), the secondary induced voltage decreases, and zero offset increases.

2) Zero drift is related to frequency, matching capacitance, and the inductance of the second magnetic core. The lower the frequency, the fewer components are filtered out by the matching capacitance, and the larger the zero drift. The larger the inductance of the second magnetic core, the more components are filtered out, and the smaller the zero offset. When Hs is constant, as L increases, the magnetic core becomes more difficult to saturate, the frequency decreases, fewer components are filtered by the matching capacitance, and zero drift eventually increases.When the magnetic flux is constant, as Hs increases, the frequency increases and zero drift decreases.When L is constant, as Hs and Ms increase, the magnetic core becomes more difficult to saturate, the frequency decreases (with L unchanged), fewer components are filtered by the matching capacitance, resulting in increased zero drift.

IV. CONCLUSION

In this paper, a circuit simulation model of the magnetic core is established for a magnetic-modulation voltage sensor. The variations in zero offset and zero drift of the voltage sensor are analyzed under changes in the parameters of the magnetic-modulation core and the mutual-inductance core respectively, and corresponding laws are summarized, providing effective theoretical guidance for the design of high-precision magnetic-modulation voltage sensors.

The above simulation studies fixed the second magnetic core and varied the first one to analyze its influence on zero offset and zero drift. In practice, the second core must match the first one (the second core has little effect on zero offset, but zero drift varies with the second core). Therefore, in future work, it is necessary to establish a more accurate circuit model of the magnetic core and conduct in-depth simulation analysis. This part will be investigated in subsequent research.

REFERENCES

[1] H. J. Mou, et al., “Design and implementation of double isolation high voltage sensor based on zero flux,” Chin. J. Sens. Actuat., vol. 37, no. 2, pp. 183–188, 2024.

[2] P. H. Yao, et al., “Current and voltage detection based on magneto optical crystal fiber senor,” Laser & Optoelectronics Progress, vol. 62, no. 19, p. 1906029, 2025. DOI: 10.3788/lop62.1906029.

[3] K. Wang, et al., “A dual-core wide bandwidth and high-accuracy fluxgate current sensor,” IEEE Sens. J., vol. 26, no. 5, pp. 6929–6930, 2026. DOI: 10.1109/JSEN.2026.3567899.

[4] A. V. Lalwani, et al., “Hall-effect sensor technique for no induced voltage in AC magnetic field measurements without current spinning,” IEEE Sens. J., vol. 22, no. 2, pp. 1245–1251, 2021. DOI: 10.1109/JSEN.2021.3024567.

[5] T. T. Fan, et al., “Investigation of loss and noise in toroidal core current sensors,” J. Magn. Magn. Mater., vol. 640, p. 173788, 2026. DOI: 10.1016/j.jmmm.2025.173788.

[6] X. Y. Tan, et al., “Insulator-integrated voltage-current sensor based on electric field coupling and tunneling magnetoresistance technology,” Energies, vol. 18, p. 6296, 2025. DOI: 10.3390/en18136296.

[7] X. L. Ye, Z. S. Wang, and S. R. Wang, “Data-drived voltage control in isolated AC microgrids subject to sensor saturation,” Appl. Sci., vol. 15, no. 13, p. 7119, 2025. DOI: 10.3390/app15137119.

[8] H. Niakan, A. Farahani, and B. Parkhideh, “Galvanically isolated coreless peak current detector for switch mode power supplies,” IEEE Trans.Power Electron., pp. 1–3, 2026.

[9] J. K. Gong, et al., “Overcurrent protection enabled by broadband rogowski coil current sensor for medium-voltage SiC MOSFET, ” IEEE Trans. Power Electron., vol. 40, no. 5, pp. 6874–6859, 2025. DOI: 10.1109/TPEL.2024.3498762.

[10] J. K. Song, et al., “Design and simulation of a magnetic balance weak current sensor based on TMR,” J. Phys. Conf. Ser., vol. 1617, p. 012038, 2020. DOI: 10.1088/1742-6596/1617/1/012038.

[11] D. C. Ni, et al., “Modeling and simulation of magnetic balance current sensor based on magnetic scalar potential volume integral,” Electron., vol. 11, no, 19, p. 3008, 2022. DOI: 10.3390/electronics11193008.

[12] X. G. Yang, et al., “Unidirectional saturation in closed-Loop self-oscillating fluxgate current sensors: analysis, recovery method, and circuit design,” IEEE Sens. J., p. 1, 2026.

[13] Y. T. Liu, Y. Tao, and C. F. Ye, “Measurement of transformer DC bias current based on integrated array magnetoresistance sensors and signal fusion algorithm,” IEEE Sens. J., vol. 25, no. 7, pp. 10860–10867, 2025. DOI: 10.1109/JSEN.2025.3476123.

[14] Y. Liu, et al., “A high accuracy fluxgate DC current sensor applicable to two-wire electric appliances”, Microsyst. Technol., vol. 25, no. 3, pp. 877–885, 2019. DOI: 10.1007/s00542-018-4176-7.

[15] B. Gojdka, et al., “AMR sensor with substrate-integrated powder MEMS permanent magnets for in-plane biasing,” IEEE Sens. J., vol. 25, no. 21, pp. 39289–39295, 2025. DOI: 10.1109/JSEN.2025.3507112.
[16] Y.S Wang, et al., “GHz-bandwidth twin-coil magnetic current Ssensors for compact switching circuits,” IEEE Trans. Power Electron., vol. 14, no. 6, pp. 8910–8926, 2026.
[17] H. J. Peng, et al., “Design and simulation test of non-contact voltage sensor,” Sensors, vol. 25, no. 10, p. 3118, 2025. DOI: 10.3390/s25103118.
[18] H. Li, Y. C. Hao, and H. L. Chang, “Heat-sensitive mode-localized current sensor with ultra-high sensitivity,” Sci. China Inf. Sci.,vol. 69, no. 1, p. 112404, 2026. DOI: 10.1007/s11432-025-4587-9.
[19] X. M. Gao, et al., “Analytical model for precise parasitic capacitance assessment in current sensors with NiZn cores,” J. Phys. Conf. Ser., vol. 3046, no. 1, p. 012022, 2025. DOI: 10.1088/1742-6596/3046/1/012022.
[20] K. Xiong, et al., “Modeling and measurement of a self-oscillating fluxgate current sensor for AC and DC application,” IEEE Access, vol. 13, pp. 86430–86437, 2025. DOI: 10.1109/ACCESS.2025.3570234.
[21] H. B. Li, et al., “Analysis on the zero offset of a microampere DC current sensor using the open-loop magnetic modulator and the suppression,” IEEE Sens. J., vol. 22, no. 19, pp. 18418–18427, 2022. DOI: 10.1109/JSEN.2022.3195448.